# Disentangling factors governing Dzyaloshinskii domain-wall creep in Co/Ni thin films using $Pt_xIr_{1-x}$ seed layers

D. Lau,[1] J. P. Pellegren,[1] H. T. Nembach,[2] J. M. Shaw,[2] and V. Sokalski[1,*]

[1]*Department of Materials Science & Engineering, Carnegie Mellon University, Pittsburgh, Pennsylvania 15213, USA*

[2]*Quantum Electromagnetics Division, National Institute of Standards and Technology, Boulder, Colorado 80305, USA*

(Received 14 August 2018; revised manuscript received 10 October 2018; published 9 November 2018)

We characterize asymmetric growth of magnetic bubble domains in perpendicularly magnetized Co/Ni multilayers grown on $Pt_xIr_{1-x}$ seed layers by application of perpendicular and in-plane magnetic fields. Using a refined model of domain wall creep that incorporates contributions from the anisotropic elastic energy, $\varepsilon$, and a chirality-dependent prefactor, $v_0$, we elucidate factors that govern the mobility of Dzyaloshinskii domain walls as a function of seed-layer composition. The interfacial Dzyaloshinskii-Moriya interaction (DMI) magnitude is found to decrease monotonically with $x_{Ir}$, which is independently confirmed by Brillouin light scattering. Moreover, the persistence of significant asymmetry in velocity curves across the full composition range supports previous assertions that a chirality-dependent attempt frequency akin to chiral damping could play a critical role in the observed trends. This work helps resolve fundamental questions about the factors governing Dzyaloshinskii domain-wall creep and demonstrates varying Pt-Ir seed-layer composition as a method to tune DMI.

DOI: 10.1103/PhysRevB.98.184410

## I. INTRODUCTION

Recent observations that topologically protected magnetic features like skyrmions and chiral domain walls (DWs) can be manipulated with spin current has renewed interest in developing spintronic devices for energy efficient nonvolatile memory and logic applications [1–6]. These topological structures are stabilized by the Dzyaloshinskii-Moriya Interaction (DMI), which is an antisymmetric exchange energy that scales as $E = -\mathbf{D} \cdot (\mathbf{S}_1 \times \mathbf{S}_2)$, leading to chiral winding configurations as the ground state [7,8]. Here, $\mathbf{S}$ represents the spin angular momentum of neighboring electrons and $\mathbf{D}$ is the DMI vector. Prospects for future thin-film engineering in this area were bolstered by the discovery of an interfacial DMI (iDMI) that exists in ultrathin heavy metal/ferromagnet heterostructures because of their structural inversion asymmetry (SIA) [9]. In this case, $\mathbf{D}$ is restricted to lie in the plane of the film with direction given by $\mathbf{D} = D(\hat{r} \times \hat{z})$, where $\hat{r}$ and $\hat{z}$ are the unit vectors from $\mathbf{S}_1$ to $\mathbf{S}_2$ and the film normal, respectively. The impact of several seed layers and their thickness have been explored experimentally in an effort to control the strength of this effect [10–14]. However, to date there have only been theoretical investigations on the composition dependence of the iDMI, which we present here for Pt-Ir alloys [15]. In thin films with a perpendicular magnetization, $\mathbf{D}$ can be described by an effective field, $\mu_o H_{\mathrm{DMI}} = D/(M_s\lambda)$, that acts on the internal magnetization of a DW favoring the Néel configuration over the in the out-of-plane geometry magnetostatically favored Bloch type, where $M_s$ and $\lambda$ are the saturation magnetization and Bloch wall width, respectively [10,11,16]. It is now well established that the combination of $H_{\mathrm{DMI}}$ and an in-plane field $H_x$ leads to a wall energy that is highly anisotropic with respect to the DW normal's spatial orientation about $H_x$ [17–19]. This break in symmetry results in asymmetric expansion of magnetic bubble domains when subjected to a perpendicular driving field [10,11,20,21]. For small driving fields, the motion is thermally activated with velocity described by the Arrhenius creep scaling law, $v = v_o e^{\zeta H_z^{-1/4}}$, where $\zeta$ has built in the activation energy for DW propagation and is proportional to the fourth root of the DW elastic energy, $\varepsilon^{1/4}$. The prefactor, $v_0$, is the corresponding attempt frequency for DW propagation [22,23]. Although asymmetric domain growth has become the predominant technique for extracting $D$, fundamental questions remain about how to interpret creep velocity changes with $H_x$ in ultrathin ferromagnetic films with appreciable iDMI.

## II. MODIFIED DISPERSIVE STIFFNESS MODEL FOR DW CREEP

Initial work on this topic suggested that $\varepsilon$ is equivalent to $\sigma$, the wall energy, and was the factor governing DW velocity. Assuming constant $\lambda$, $\sigma$ vs $H_x$ is symmetric about a maximum that occurs when $H_x = H_{\mathrm{DMI}}$ and was proposed to correspond to a minimum in velocity [10,11]. Significant asymmetric deviations from this idealized shape observed experimentally led to speculation about other possible factors that could be contributing [21,24–26]. This included chiral damping, which would impact $v_0$ instead of $\varepsilon$ and depends only on the orientation of the DW internal magnetization [25]. It was also later identified that $\varepsilon$ is actually given by the stiffness, $\tilde{\sigma}(\Theta) = \sigma(\Theta) + \sigma''(\Theta)$, which should reside in the exponent of the creep law instead of $\sigma(\Theta)$ [19]. Here $\Theta$ denotes the angle between the DW normal and $H_x$. In the isotropic case, $\sigma''(\Theta) = 0$. However, in cases of anisotropic DW energy as

*vsokalsk@andrew.cmu.edu

 

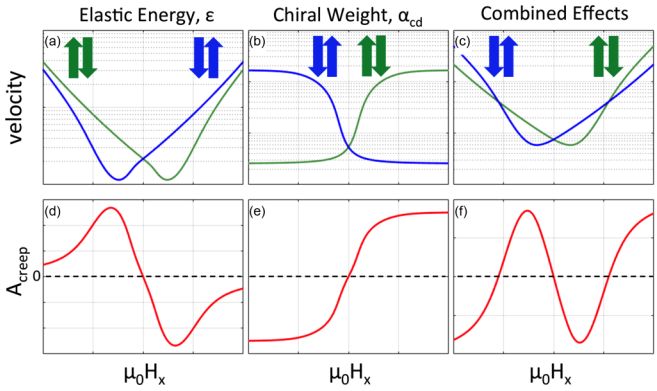


FIG. 1. Illustration of the impact of the anisotropic elastic energy (a) and chiral weight (b) on velocity vs $\mu_0 H_x$ with their combined effect shown in (c). (d)–(f) The corresponding effects on $A_{creep}$. Most notable is the convergence of ↑↓ (blue) and ↓↑ (red) domain walls at large $\mu_0 H_x$ for the case of elastic energy alone. This convergence is absent for a nonzero chiral weight.

found in Dzyaloshinskii DWs subject to $H_x$ here, $\sigma''(\Theta)$ becomes comparable in magnitude $\sigma(\Theta)$. This description based only on elastic energy of the DW demonstrated that significant curve asymmetry should exist due exclusively to iDMI and was able to explain some of the perplexing experimental data.

In this paper, we use an augmented model for Dzyaloshinskii DW creep to fit experimental measurements of asymmetric domain growth in Co/Ni multilayers grown on Pt-Ir alloy seed layers. The model incorporates elastic energy of the DW based on its dispersive stiffness [19] and also allows for an empirical chirality-dependent prefactor given by $v_0(H_x) = v_0^*(1 + \alpha_{cd}\cos(\phi_{eq}(H_x) - \Theta))$, where $\alpha_{cd}$ is a parameter from $f$-1 to 1 that characterizes the weight of this effect—hereafter referred to as the chiral weight. $\phi_{eq}$ is the equilibrium internal magnetization orientation with respect to $H_x$ as calculated in Pellegren *et al.* [19] $v_0^*$ is the attempt frequency absent any chiral effects. Importantly, we note that a field-dependent prefactor has also been proposed to originate from changes in the depinning field (which will in turn depend on $H_x$) [27] and made more complicated by the inherent roughness of magnetic DWs [28]. Although such dependence is also likely in the present system, it is not clear if the depinning field will depend explicitly on the internal magnetization direction; a criterion necessary for $A_{creep}$ to saturate as seen in our experimental results to follow.

For calculations of $v_0$, we only consider the case of $\Theta = 0$ or $\pi$ to account for fits to the left and right velocities of the bubble domains. The resulting creep equation describing DW velocity as a function of $H_x$ is given as follows:

$$v = v_0(H_x)\exp\left[\kappa \frac{\tilde{\sigma}(H_x)}{\tilde{\sigma}(H_x = 0)} H_z^{-1/4}\right], \quad (1)$$

where $\kappa$ is a creep scaling constant that does not depend on $H_x$. $\tilde{\sigma}$ is calculated using the dispersive stiffness model of Pellegren *et al.* in the limit of a vanishingly small deformation length scale, $L$ as justified later [19]. The effects of elastic energy and chiral weight on the shape of velocity curves is shown qualitatively in Fig. 1. The asymmetric component, $A_{creep} = \ln(v_{\uparrow\downarrow}/v_{\downarrow\uparrow})$, is included to further highlight experimental signatures associated with the different mechanisms. ($v_{\uparrow\downarrow}$ and $v_{\downarrow\uparrow}$ are the DW velocities, where the magnetization transitions from up to down and down to up, respectively. In the case where only elastic energy is considered, $v_{\uparrow\downarrow}$ and $v_{\downarrow\uparrow}$ converge (i.e., $A_{creep} = 0$) as $H_x \to \infty$. For a nonzero $\alpha_{cd}$, $A_{creep}$ saturates when $H_x > H_{DMI} + H_{DW}$, where $H_{DW}$ is the DW anisotropy field.

## III. EXPERIMENTAL

Co/Ni films were prepared using DC magnetron sputtering from 5-in targets onto 3-in Si (001) substrates with native oxide. The working pressure was fixed at 2.5 mTorr Ar. The film stack is Substrate/TaN(3)/Pt(3.5)/$Pt_xIr_{1-x}$(1.2)/[Co(0.2)/Ni(0.6)]$_2$/Co(0.2)/Ta(0.8)/TaN(6), with units in nanometers. The $Pt_x$-$Ir_{1-x}$ seed layer is prepared using a combinatorial sputtering technique where the substrate is moved between two targets rapidly, depositing <0.05 nm of material in each cycle to mimic the cosputtering process. This results in a linear composition gradient across the substrate surface.

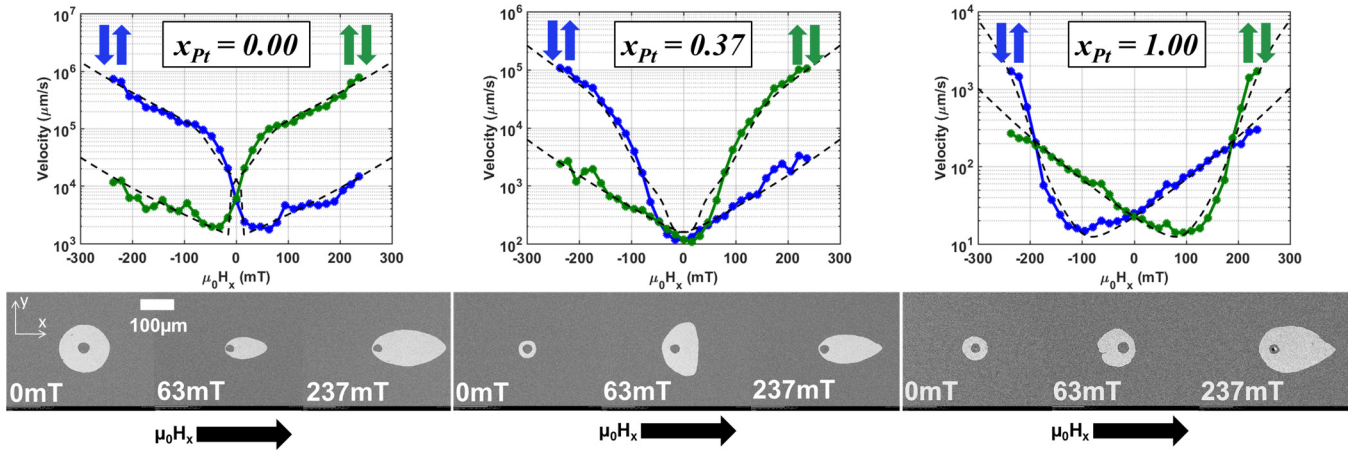


FIG. 2. Experimental v vs $\mu_0 H_x$ for seed layers with varying $x_{Pt}$ with representative MOKE images. Dashed lines are fits from Eq. (1). The center grey of the Kerr images represent the initial bubble shape while the white region is the domain after growth under both $\mu_0 H_x$ and $\mu_0 H_z$, which was fixed at 7 mT.

Details on the structural characterization of similar Co/Ni multilayer films can be found in Ref. [29]. $M-H$ loops measured using alternating gradient field magnetometry and vibrating sample magnetometry across the composition gradient indicate a saturation magnetization, $M_s \sim 645\,\mathrm{kA/m}$, and in-plane saturation field, $\mu_0 H_k \sim 1.3\,\mathrm{T}$, which has little dependence on $Pt_xIr_{1-x}$ seed-layer composition [30]. Measurement of domain growth was performed using a wide-field white light Kerr microscope. The microscope is fit with an in-plane electromagnet capable of producing static in-plane fields up to $\mu_0 H_x \sim 250$ mT as well as a perpendicular coil that can generate up to $\mu_0 H_p \sim 20$ mT magnetic pulses down to 1 ms. As described in Refs. [17,19], a $Ga^+$ ion beam is used to selectively damage portions of a sample film, where initial bubble domains of approximately 20 $\mu$m can be nucleated. Velocity was determined by two images showing the difference in domain wall positions before and after a single pulse. The pulse length ranged from 1–20 ms and was chosen so that an appreciable displacement would occur.

We used Brillouin light scattering spectroscopy (BLS) to establish an independent measure of the magnitude of the DMI. The laser had a wavelength of 532 nm. Damon-Eshbach spin waves experience a nonreciprocal frequency-shift $\Delta f_{\mathrm{DMI}} = |\frac{g^{||}\mu_B}{h}|\mathrm{sgn}(M)\frac{2D}{M_s}k$ in the presence of DMI. The spectroscopic splitting factor is estimated as $g^{||} = 2.19$ [31], $\mu_B$ is the Bohr Magneton, h is Planck's constant and **k** is the spin-wave wave vector with $|k| = 16.7\ \mu\mathrm{m}^{-1}$. We measured the spin-wave frequency for the two opposite directions of the magnetization to determine $\Delta f_{\mathrm{DMI}}$. The measured $|\Delta f_{\mathrm{DMI}}|$ was between 0.1 GHz and 0.8. GHz

## IV. RESULTS & DISCUSSION

Figure 2 shows representative Kerr images as a function of in-plane field ($H_x$) and seedlayer composition with corresponding $v$ vs $H_x$ curves. As seen in previous studies, the domain shape is highly nonelliptical, evolving from a flattened shape at low field to a teardrop shape at higher field [4,17,21]. The field at which this occurs is found to be directly related to the amount of Pt in the seed layer (see Supplemental Material for additional Kerr images [30]). To separate the effects of elastic energy and chiral weight, we examine the shape of $v$ vs $H_x$ and the calculated $A_{\mathrm{creep}}$ (Fig. 3). In all cases, the velocity curve is asymmetric about a minimum in velocity. This leads to a reversal in the preferred expansions direction in the Pt-rich compositions, which is indicated by the intersection of the velocity curves in Fig. 2 and by the zero crossing of $A_{\mathrm{creep}}$ in Fig. 3(a). As identified previously, a change in sign of $A_{\mathrm{creep}}$ at nonzero $H_x$ could be explained using a larger deformation length scale, L, in the dispersive stiffness model [19]. However, the observation that $A_{\mathrm{creep}}$ tends to saturate rather than return to zero suggests this is not the case. Therefore, we limit our fitting to the case of $L \to 0$, which is consistent with the expectation that pinning sites in sputtered thin films are densely distributed. We note that as the composition shifts from $x_{Pt} = 1$ to 0, the minimum in velocity shifts toward $H_x = 0$ and changes sign near $x_{Pt} = 0.25$. However, as the creep fits and BLS measurements show, $D$ does not actually change sign and only approaches 0 for the case of pure Ir. This result is in stark contrast to the aforementioned creep models

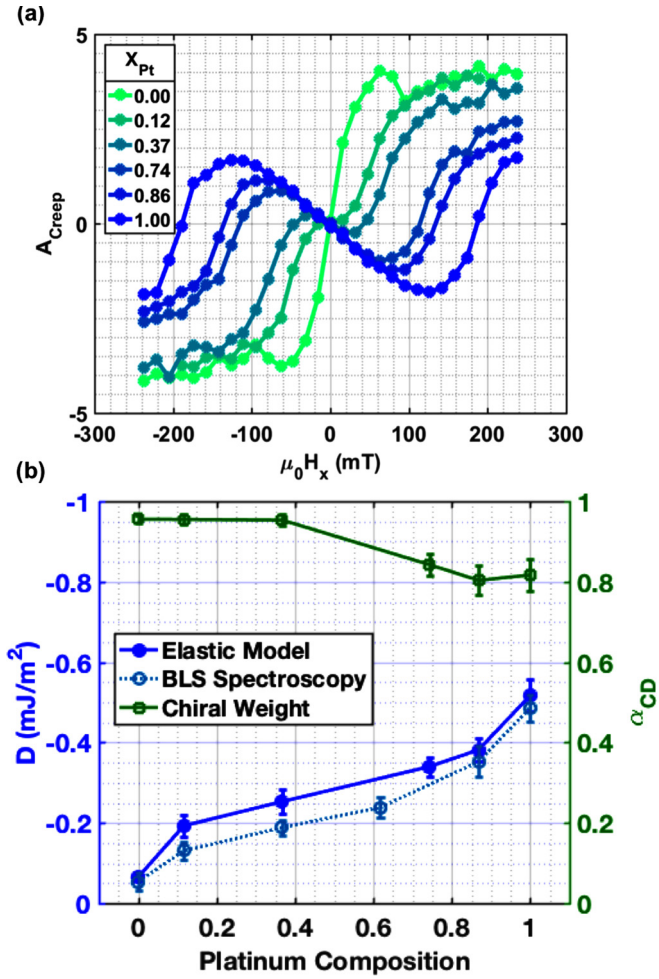


FIG. 3. (a) $A_{\mathrm{creep}}$ vs $\mu_0 H_x$ as a function of $X_{Pt}$. (b) Extracted values of $D$ and $\alpha_{\mathrm{cd}}$ vs $X_{Pt}$ based on fits to $A_{\mathrm{creep}}$. Closed blue (dark) circles represent fits extracted from the elastic domain wall model. Open blue (light) circles represent $D$ values characterized using BLS demonstrated by Nembach *et al.* [12].

based only on the wall energy, which would have given the incorrect sign of $D$ in this range [10,11].

Even as $D$ decreases with decreasing $x_{Pt}$, the asymmetry of the curve is preserved, suggesting that its origin is not exclusively due to iDMI. Indeed, $A_{\mathrm{creep}}$ appears to saturate in all cases, even though its magnitude is reduced for increasing Pt content. The results of the fit to the velocity curves are shown in Fig. 3(b), highlighting that significant $\alpha_{\mathrm{cd}}$ is needed to explain the data of Figs. 2 and 3(a), and dominates the trend for large $X_{Ir}$.

To further examine the impact of chiral weight and iDMI via the elastic energy, we have prepared the following films: TaN(3)/Pt(2.5)/$[$Co(0.2)/Ni(0.6)$]_2$/Co(0.2)/Ir(2.5)/TaN(6) and the same stack with Pt and Ir positions swapped. These are referred to as Pt-seed/Ir-cap and Ir-seed/Pt-cap, respectively. Velocity curves and asymmetry for these samples are shown in Fig. 4. We note that the magnitude of $D$ measured here should not be compared with the results tabulated in Fig. 3 because we have significantly increased the effective magnetic layer thickness by replacing the Ta cap (known to create a magnetic dead layer) with either Pt or Ir (both known to have a

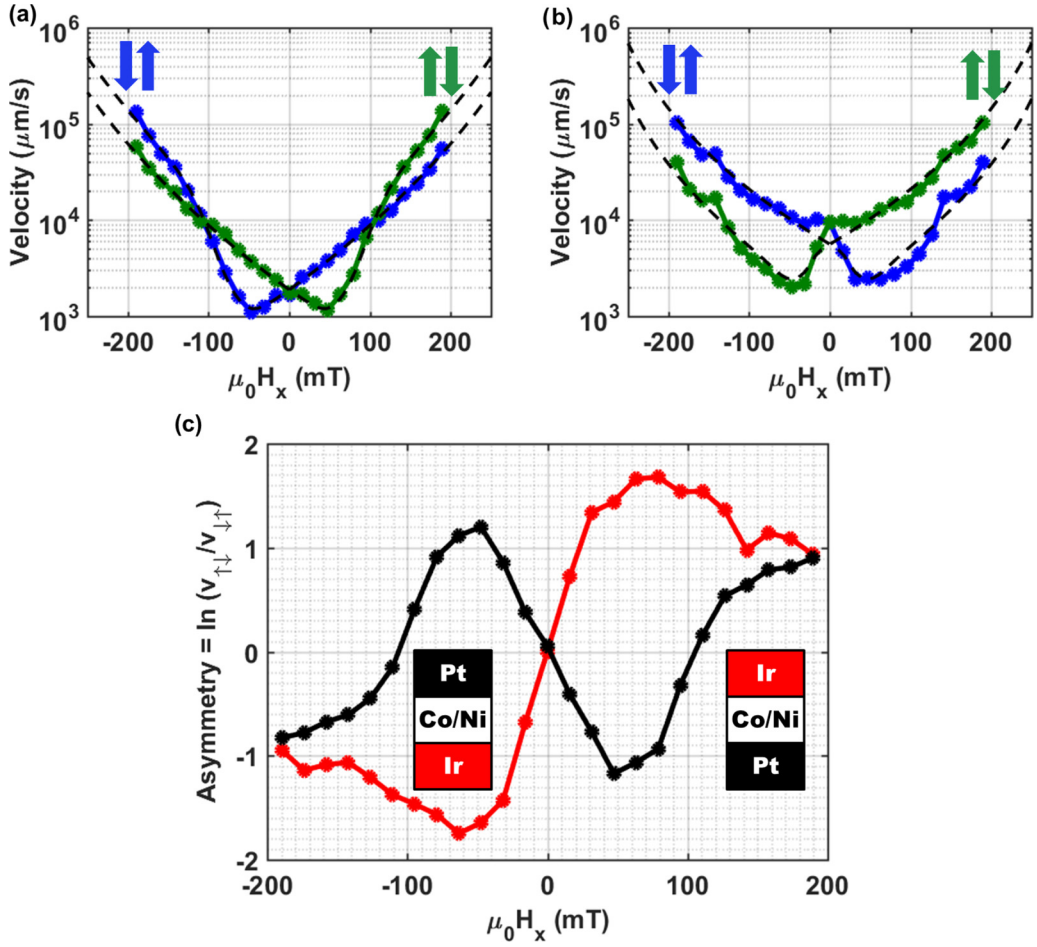


FIG. 4. Experimental velocity vs $\mu_0 H_x$ for samples grown with (a) Pt seed layer/Ir capping layer and (b) Ir seed layer/Pt capping layer. (c) $A_{\text{creep}}$ vs $\mu_0 H_x$ calculated from experimental velocity data in (a) and (b).

proximity induced magnetization). Indeed, we see that the sign of $D$ is reversed between these two cases with comparable magnitudes as expected. The Pt seed/Ir cap favors left-handed Néel walls ($D = -0.313 \pm 0.009\,\text{mJ/m}^2$) and the Ir seed/Pt cap favors right-handed Néel walls ($D = 0.214 \pm 0.020\,\text{mJ/m}^2$). It is interesting that despite the expected change in sign of $D$, $\alpha_{\text{cd}}$ remains nearly the same ($\alpha_{\text{cd},Pt-\text{seed}} = 0.41 \pm 0.04$, $\alpha_{\text{cd},Ir-\text{seed}} = 0.58 \pm 0.07$). If $\alpha_{\text{cd}}$ depended exclusively on the elements present and interface orientation, we should see a change in sign upon reversal of the film stack. The absence of this reversal suggests that there could be a contribution to the chiral weight that is intrinsic to the Co/Ni stack even though it is nominally symmetric. Just as Pt/Co/Pt films are known to have SIA, it is conceivable that the Co/Ni/Co/Ni/Co film stack itself could be structurally asymmetric if the lattice evolves through the thickness and/or the top and bottom Co/Ni interfaces are not identical. This assertion requires further investigation as it is also possible that the chiral weight contributions from Pt and Ir change when used as seed vs cap layers.

## V. CONCLUSION

In summary, we have shown a monotonic increase of $D$ with $X_{Pt}$ in $Pt_xIr_{1-x}$ seed-layer alloys. Moreover, we show that the impact of DMI on elastic energy is insufficient to explain the trends in velocity curves seen experimentally. The results are fit well only when a chirality-dependent attempt frequency is included in the model—something speculated to originate from chiral damping or, more recently, a chiral gyromagnetic ratio [25,32]. However, it remains unclear if the 10–100x increase in velocity seen here is consistent with these mechanisms. We also show definitively that reversal of Pt and Ir stack sequence indeed reverses the sign of $D$, but does not change the sign of $\alpha_{\text{cd}}$. This suggests that there could be a mechanism for chiral effects built into the Co/Ni multilayers themselves. The ability to tune iDMI via Pt-Ir composition and through reversal of Pt:Ir stacking sequence as demonstrated here provides new guidance for the design of film stacks in future spintronic applications.

## ACKNOWLEDGMENTS

This work has been funded by the DARPA Topological Excitations in Electronics (TEE) program under Grants No. D18AP00011 and No. R186870004. It was also funded (in part) by the Dowd Fellowship from the College of Engineering at Carnegie Mellon University. The authors would like to thank Philip and Marsha Dowd for their financial support and encouragement as well as Emilie Jué for her help with the BLS data analysis.

[1] D. M. Bromberg, M. T. Moneck, V. M. Sokalski, J. Zhu, L. Pileggi, and J. G. Zhu, in *2014 IEEE International Electron Devices Meeting* (IEEE, 2014), pp. 33.1.1–33.1.4.

[2] S. Emori, U. Bauer, S.-M. Ahn, E. Martinez, and G. S. D. Beach, Nat. Mater. **12**, 611 (2013).

[3] K.-S. Ryu, S.-H. Yang, L. Thomas, and S. S. P. Parkin, Nat. Commun. **5**, 3910 (2014).

[4] S. Woo, K. Litzius, B. Krüger, M.-Y. Im, L. Caretta, K. Richter, M. Mann, A. Krone, R. M. Reeve, M. Weigand *et al.*, Nat. Mater. **15**, 501 (2016).

[5] M. Heide, G. Bihlmayer, and S. Blügel, Phys. Rev. B **78**, 140403 (2008).

[6] S. Heinze, K. von Bergmann, M. Menzel, J. Brede, A. Kubetzka, R. Wiesendanger, G. Bihlmayer, and S. Blugel, Nat. Phys. **7**, 713 (2011).

[7] I. Dzyaloshinsky, J. Phys. Chem. Solids **4**, 241 (1958).

[8] T. Moriya, Phys. Rev. **120**, 91 (1960).

[9] A. Thiaville, S. Rohart, É. Jué, V. Cros, and A. Fert, Europhys. Lett. **100**, 57002 (2012).

[10] A. Hrabec, N. A. Porter, A. Wells, M. J. Benitez, G. Burnell, S. McVitie, D. McGrouther, T. A. Moore, and C. H. Marrows, Phys. Rev. B **90**, 020402(R) (2014).

[11] S.-G. Je, D.-H. Kim, S.-C. Yoo, B.-C. Min, K.-J. Lee, and S.-B. Choe, Phys. Rev. B **88**, 214401 (2013).

[12] H. T. Nembach, J. M. Shaw, M. Weiler, E. Jue, and T. J. Silva, Nat. Phys. **11**, 825 (2015).

[13] R. Soucaille, M. Belmeguenai, J. Torrejon, J.-V. Kim, T. Devolder, Y. Roussigné, S.-M. Chérif, A. A. Stashkevich, M. Hayashi, and J.-P. Adam, Phys. Rev. B **94**, 104431 (2016).

[14] M. Vaňatka, J.-C. Rojas-Sánchez, J. Vogel, M. Bonfim, M. Belmeguenai, Y. Roussigné, A. Stashkevich, A. Thiaville, and S. Pizzini, J. Phys.: Condens. Matter **27**, 326002 (2015).

[15] J.-P. Hanke, F. Freimuth, S. Blügel, and Y. Mokrousov, J. Phys. Soc. Jpn. **87**, 041010 (2018).

[16] G. Chen, T. P. Ma, A. T. N'Diaye, H. Kwon, C. Won, Y. Z. Wu, and A. K. Schmid, Nat. Commun. **4**, 2671 (2013).

[17] D. Lau, V. Sundar, J.-G. Zhu, and V. Sokalski, Phys. Rev. B **94**, 060401(R) (2016).

[18] E. Martinez, S. Emori, N. Perez, L. Torres, and G. S. D. Beach, J. Appl. Phys. **115**, 213909 (2014).

[19] J. P. Pellegren, D. Lau, and V. Sokalski, Phys. Rev. Lett. **119**, 027203 (2017).

[20] Y. P. Kabanov, Y. L. Iunin, V. I. Nikitenko, A. J. Shapiro, R. D. Shull, L. Y. Zhu, and C. L. Chien, IEEE Trans. Magn. **46**, 2220 (2010).

[21] R. Lavrijsen, D. M. F. Hartmann, A. van den Brink, Y. Yin, B. Barcones, R. A. Duine, M. A. Verheijen, H. J. M. Swagten, and B. Koopmans, Phys. Rev. B **91**, 104414 (2015).

[22] G. Blatter, M. V. Feigel'man, V. B. Geshkenbein, A. I. Larkin, and V. M. Vinokur, Rev. Mod. Phys. **66**, 1125 (1994).

[23] S. Lemerle, J. Ferré, C. Chappert, V. Mathet, T. Giamarchi, and P. Le Doussal, Phys. Rev. Lett. **80**, 849 (1998).

[24] C. A. Akosa, I. M. Miron, G. Gaudin, and A. Manchon, Phys. Rev. B **93**, 214429 (2016).

[25] E. Jué, C. K. Safeer, M. Drouard, A. Lopez, P. Balint, L. Buda-Prejbeanu, O. Boulle, S. Auffret, A. Schuhl, A. Manchon, I. M. Miron, and G. Gaudin, Nat. Mater. **15**, 272 (2016).

[26] D.-Y. Kim, D.-H. Kim, and S.-B. Choe, Appl. Phys. Express **9**, 053001 (2016).

[27] V. Jeudy, A. Mougin, S. Bustingorry, W. Savero Torres, J. Gorchon, A. B. Kolton, A. Lemaître, and J.-P. Jamet, Phys. Rev. Lett. **117**, 057201 (2016).

[28] P. M. Shepley, H. Tunnicliffe, K. Shahbazi, G. Burnell, and T. A. Moore, Phys. Rev. B **97**, 134417 (2018).

[29] M. Jaris, D. Lau, V. Sokalski, and H. Schmidt, J. Appl. Phys. **121**, 163903 (2017).

[30] See Supplemental Material at http://link.aps.org/supplemental/10.1103/PhysRevB.98.184410 for additional magnetic property measurements.

[31] M. Arora, R. Hübner, D. Suess, B. Heinrich, and E. Girt, Phys. Rev. B **96**, 024401 (2017).

[32] K.-W. Kim, H.-W. Lee, K.-J. Lee, K. Everschor-Sitte, O. Gomonay, and J. Sinova, Phys. Rev. B **97**, 100402 (2018).